ACS SENSORS

pubs.acs.org/acssensors Article

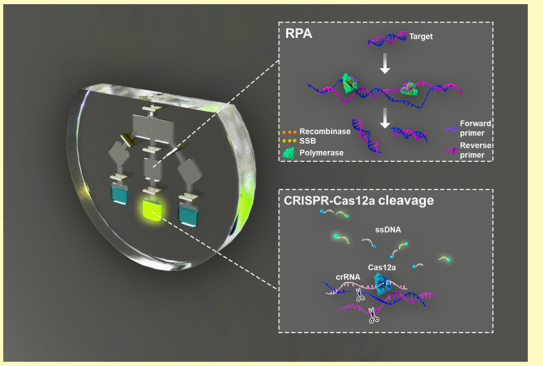
# Multiple-Channel Funnel Adapted Sensing Tube (MFAST) for the Simple and Duplex Detection of Parasites

Ruonan Peng,[▽] FNU Yuqing,[▽] Taralyn J. Wiggins, Negin Bahadori, Joshua S. Rogers, Jacob Waitkus, Yun Chen, Gregory J. Tobin, Stephen J. Dollery,* and Ke Du*

Cite This: https://doi.org/10.1021/acssensors.4c03306 Read Online

ACCESS | Metrics & More | Article Recommendations | Supporting Information

**ABSTRACT:** Leishmaniasis poses a significant global health threat, infecting millions of people annually, particularly in tropical and subtropical regions. Timely and accurate detection of the *Leishmania* species is crucial for effective treatment and control of this debilitating disease. This study introduces the multi-channel funnel adapted sensing tube (MFAST) chip, a simple diagnostic tool designed for the rapid detection of *Leishmania panamensis*. MFAST is fabricated through 3D printing and sacrificial molding of acrylonitrile butadiene styrene (ABS) and the reagents are transported between reservoirs by gravity. We combine experiments and finite element analysis to facilitate smoother fluid flow, improving the overall performance of the device. Highly sensitive and specific RPA-CRISPR/Cas12a assay is utilized in the chip, achieving a detection limit as low as 1000 parasites/mL (detecting as few as 5 parasites per reaction). The multichannel design enables duplex detection, allowing for simultaneous identification of both *L. braziliensis* and *L. panamensis* through distinct channels. Furthermore, stability tests indicate that lyophilized reagents retain functionality for up to 15 days when stored at 4 °C, underscoring the potential of this chip for practical diagnostic applications in low-resource settings.




**KEYWORDS:** *point-of-care, parasites, CRISPR, duplex, diagnostics, fluorescence, and sacrificial molding*

Downloaded via SHANGHAI NORMAL UNIV on March 29, 2025 at 01:30:35 (UTC).
See https://pubs.acs.org/sharingguidelines for options on how to legitimately share published articles.

Leishmaniasis ranks second only to malaria among parasitic diseases in terms of mortality.[1] In 2020, 98 of the 200 countries and territories (49%) reporting to the WHO were classified as endemic for Leishmaniasis.[2] The disease is caused by the *Leishmania* parasite, a protozoan transmitted to humans through the bite of infected phlebotomine sandflies. The transmission occurs when a sandfly bites an infected person or animal and then bites another individual, injecting them with the *Leishmania* parasite.[3−5] *Leishmania* is a genus in the family Trypanosomatidae, comprising over 20 species known to cause disease in humans.[6] The disease disproportionately affects vulnerable populations, particularly in areas with malnutrition,[7] poor housing,[8] weakened immune systems,[9] and limited healthcare access.[10] There are three main forms of leishmaniasis: cutaneous leishmaniasis (CL), visceral leishmaniasis (VL), also known as kala-azar, and mucocutaneous leishmaniasis (ML).[11] While VL is the most deadly form, ML is more prevalent in the Americas and can cause severe complications, particularly through ulceration of the mucous membranes of the nose, mouth, or throat.[12−14] Mucocutaneous leishmaniasis rarely heals on its own and, if left untreated, the inflammatory process can affect all oro/naspharyngeal structures and potentially be fatal.[15] Significant facial disfigurement can occur due to the destruction of the oro/nasopharyngeal mucosa and cartilage in later stages. In severe cases, it can affect the larynx, leading to aspiration pneumonia.[16]

Early detection is crucial, especially in resource-limited settings, to enable timely medical intervention and reduce the risk of disease spread.[17] While VL is the most dangerous form of the disease, it can be diagnosed using a combination of clinical signs and parasitological or serological tests.[18] However, current clinical serological tests such as immunofluorescence indirect antibody test (IFAT) and rk39 immunochromatographic test (rk39 ICT) cannot distinguish between active and prior infection[11] and have limited value in diagnosing CL and ML due to poor antibody responses.[19] For CL and ML, diagnosis largely relies on clinical symptoms and parasitological tests, which confirm the presence of the parasite in affected tissues.[20] These tests, however, often face challenges due to limited specificity or sensitivity.[21] Nucleic acid−based approaches, such as polymerase chain reaction (PCR), offer high sensitivity but require advanced equipment and precise

Received: November 22, 2024
Revised: January 31, 2025
Accepted: March 3, 2025


© XXXX American Chemical Society

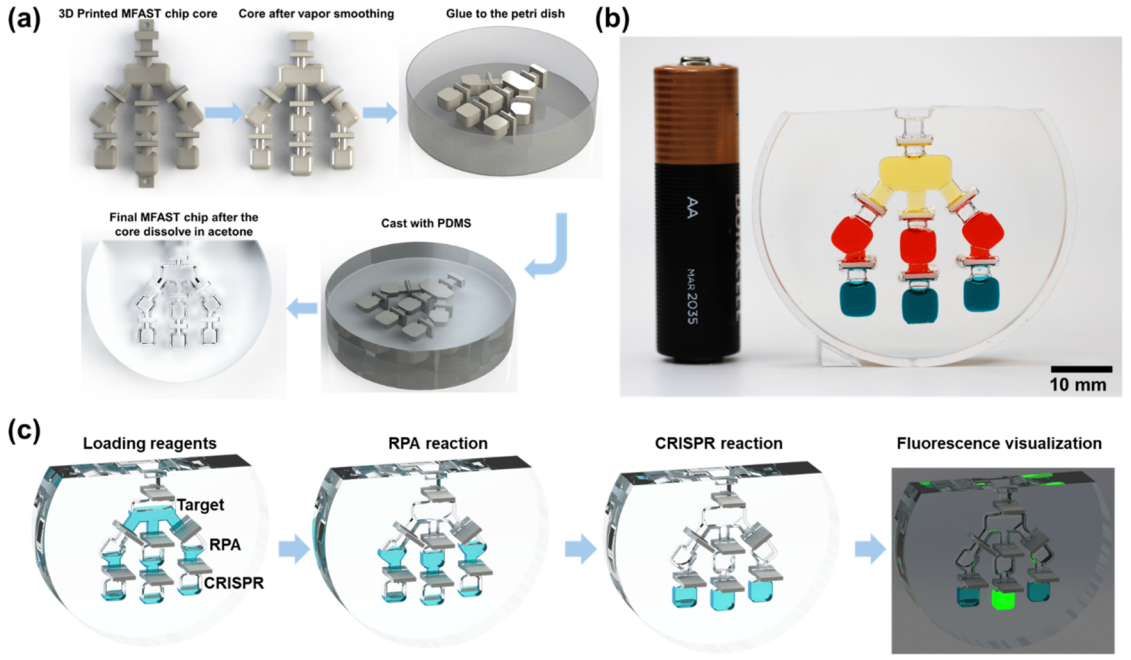



**Figure 1.** Schematic of the MFAST chip. (a) Fabrication process of MFAST chip. (b) Photograph of the MFAST chip filled with food dye and with an AA battery as a scale. (c) Working principle of the MFAST for visual detection of *Leishmania*.

thermal cycling, making them less viable for point-of-care (POC) diagnostics, especially in resource-limited settings.[22]

In recent years, clustered regularly interspaced short palindromic repeats (CRISPR)-Cas12a system has gained recognition as a promising tool for in vitro diagnostics, combining precision and simplicity in the detection of specific DNA sequences.[23] This system employs a guide RNA (crRNA) to recognize and cleave target DNA, a process known as *cis-cleavage*. Upon activation, it also engages in *trans-cleavage*, where it indiscriminately cuts nearby single-stranded DNA (ssDNA).[24] This property is utilized in diagnostic assays using ssDNA reporters tagged with a fluorophore and quencher. When Cas12a cleaves the reporter, fluorescence is generated, indicating the presence of the target DNA.[25] Unlike traditional PCR, which relies on precise thermal cycling, Cas12a operates at a constant temperature of 37 °C,[26] making it ideal for POC applications where rapid, cost-effective, and portable diagnostics are crucial.[27,28]

To enhance sensitivity, CRISPR-Cas12a is often coupled with isothermal amplification methods such as recombinase polymerase amplification (RPA), which can be performed at the same temperature.[29,30] RPA enables the rapid amplification of target DNA through the concerted actions of recombinases, single-strand binding (SSB) proteins, and DNA polymerases. The process begins when recombinases guide primers to the target DNA sequence. SSB proteins stabilize the unwound DNA strands, while DNA polymerases extend the primers along the template DNA in the presence of deoxynucleotide triphosphates (dNTPs), facilitating the synthesis of new DNA strands.[31] The RPA-CRISPR two-step process requires sequential handling to prevent premature degradation of amplified DNA and presents practical challenges. The requirement for manual pipetting between steps increases the risk of aerosol contamination, which can lead to false positives and complicate the workflow.[32] Our lab previously developed a funnel adapted sensing tube (FAST) chip that combines RPA and CRISPR reaction for power-free, pipet-free, and sensitive detection of SARS-CoV-2.[33] In the FAST chip, RPA and CRISPR reagents are stored in separate chambers and isolated by simple valves, with the reaction initiated by simply pulling the rods. This system achieved a high sensitivity of approximately 10 fM; however, the original FAST chip was single-channel, lacked negative controls on the same chip, and was unable to detect multiple strains simultaneously.

In this study, we introduce an all-in-one multi-channel funnel adapted sensing tube (MFAST) chip for the duplex detection of *Leishmania* species and specific detection of species that cause mucocutaneous leishmaniasis, such as *L. panamensis*, without cross-contamination. To achieve this, we performed vapor smoothing of the 3D-printed acrylonitrile butadiene styrene (ABS) core and applied the NeverWet coating on the valves. The combination of the two treatments increased the transport efficiency by about 25% and improved the leaking rate by over 20%. Additionally, plasma treatment of the inner surfaces further enhances hydrophilicity, allowing smoother fluid transport through gravity. The multi-channel design also enables simultaneous negative and positive control reactions within the same chip, reducing the likelihood of false positives and improving diagnostic reliability. The chip demonstrates the ability to detect *Leishmania* species with a sensitivity as low as 1000 parasites/mL (detecting as few as 5 parasites per reaction), enabled by a highly specific RPA-CRISPR/Cas12a assay. This sensitivity is sufficient for practical diagnostic applications, given that the mean parasite load in the blood of visceral leishmaniasis (VL) patients ($n$ = 31) is approximately 8372 parasites/mL.[34] By integrating a portable blue light transilluminator, this chip is operated without using pipettes, significantly simplifying on-site diagnostics. The duplex testing capability further enhances efficiency by minimizing reagent consumption and enabling the simultaneous detection of multiple species. This versatile, low-cost platform is well suited for the POC diagnosis of parasites, particularly in low-resource settings.


https://doi.org/10.1021/acssensors.4c03306
ACS Sens. XXXX, XXX, XXX−XXX

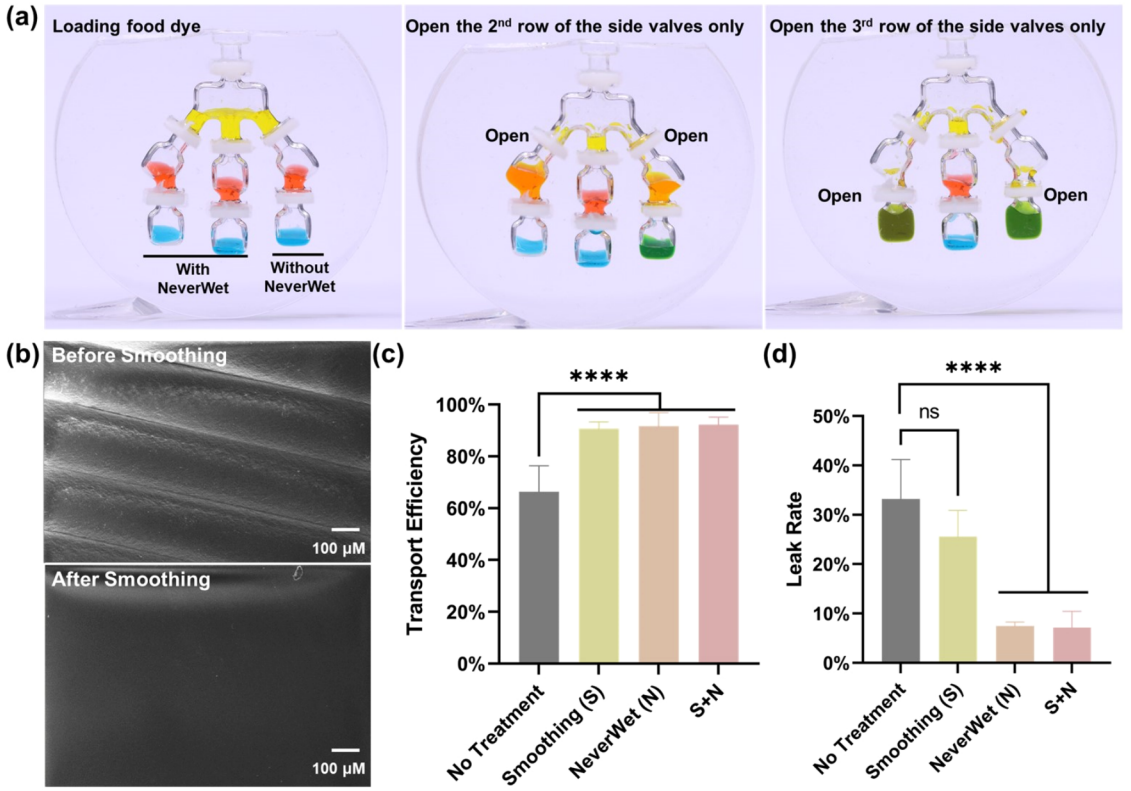



**Figure 2.** Surface treatment and quantification of MFAST chip. (a) Food dye test evaluating the leak-prevention capabilities of the NeverWet coating. The left photo illustrates the food dye loading process with all valves closed. The valves in the left and middle channels were coated with NeverWet, while the right channel remained uncoated. The middle photo depicts the mixing of food dye after opening only the second row of side valves while keeping the valves of the middle channel closed. The right photo shows the mixing of food dye after opening only the bottom row of side valves while keeping the valves of the middle channel closed. (b) SEM images of the ABS core before (top) and after (bottom) vapor smoothing. (c) Transport efficiency of the MFAST chip without treatment, with vapor smoothing of the ABS core, with NeverWet coating on the valves, and with both treatments combined. (d) Leak rate of the MFAST chip without treatment, with vapor smoothing of the ABS core, with NeverWet coating on the valves, and with both treatments combined. Statistical analyses were performed using one-way ANOVA. The data are represented as mean ± standard deviation ($n = 3$). ns, not significant = $p > 0.05$; * = $0.01 < p \leq 0.05$; ** = $0.001 < p \leq 0.01$; **** = $p \leq 0.0001$.

## RESULTS AND DISCUSSION

The fabrication process of the MFAST chip is illustrated in Figure 1a. The chip core was 3D-printed using an ABS material. To create a smooth surface, the printed core was suspended in a heated acetone vapor chamber, which dissolved surface imperfections and produced a glossy finish, enhancing the clarity of the visualization. The smoothed core was then attached to a Petri dish, and a mixture of polydimethylsiloxane (PDMS) and curing agent was poured into the mold. Once cured, the chip was submerged in acetone, dissolving the ABS core and leaving behind the final microfluidic structure. Figure 1b shows a photograph of a fabricated MFAST chip filled with food dye, which is distinctly observable by the naked eye. The chambers are delineated by 3D-printed rectangular pieces that serve as functional valves. The volumes of the chambers, from top to bottom, are around 338, 160, and 160 μL, respectively. The corners of the chambers are rounded to minimize dead volume, thereby enhancing the efficiency of reagent flow. This design modification facilitates smoother transport of reagents, ultimately improving the overall operational efficiency of the chip.

Figure 1c illustrates the visual detection process employed by the self-contained MFAST chip. Prior to the initiating reaction, RPA and CRISPR reagents were systematically loaded into the designated chambers of the MFAST chip. Specifically, 26.5 μL of the CRISPR-Cas12a complex was introduced into the bottom chambers, while a total of 68.6 μL of a mixture containing primers and a rehydrated TwistAmp basic reaction pellet was loaded into the second row of the chamber. The top chamber was filled with 75 μL of a nuclease-free water and magnesium acetate mixture, which is used to activate the RPA reaction. Once 15 μL of the target was added to the top chamber, the chip was prepared for visual detection. The amplification reaction commenced by pulling the top valves, enabling the target to flow downward and mix with the RPA reagents. After a 20 min incubation at 37 °C on a heating pad, the resulting amplicons were transferred to the CRISPR reaction chamber for an additional incubation of 30 min at the same temperature. Following this, a blue light transilluminator was utilized to excite the fluorophore, allowing for naked eye observation of the reaction results.

After the MFAST chip was fabricated, surface treatments were made to optimize its performance, including the application of a NeverWet coating on the valves and vapor smoothing of the 3D-printed core. To demonstrate the leak-prevention capabilities of the NeverWet coating, Figure 2a shows a food dye test. In the left image, the MFAST chip is loaded with yellow, red, and blue dyes in the top, middle, and bottom chambers, respectively. The valves in the left and middle channels were coated with NeverWet, while the right channel remained uncoated. In the middle image, after opening


https://doi.org/10.1021/acssensors.4c03306
ACS Sens. XXXX, XXX, XXX−XXX

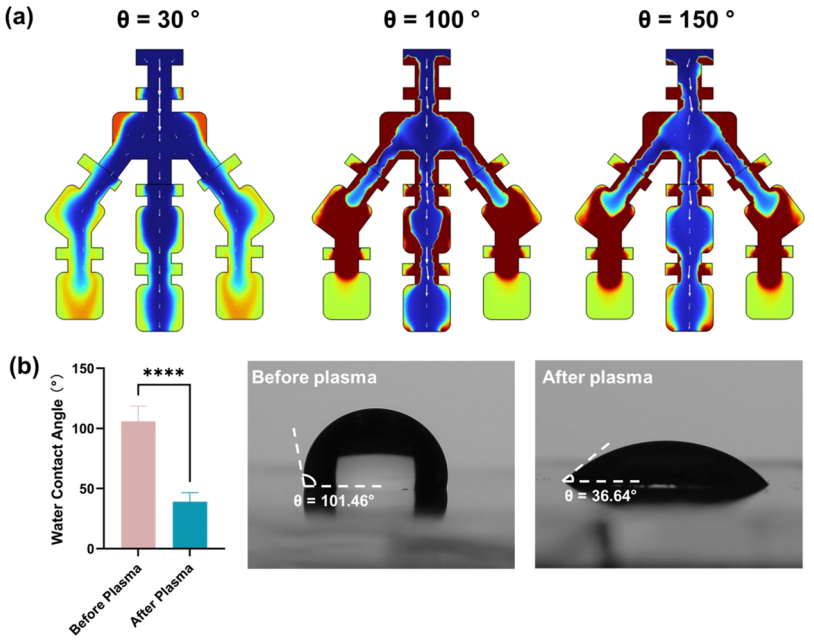



**Figure 3.** Liquid flow simulation and effect of plasma treatment on wettability. (a) Simulation results of volume fraction showing the effect of varying surface wettability at time = 6 s. (b) Static contact angles of MFAST chip before (left) and after (right) plasma treatment. Statistical analyses were performed using unpaired *t*-test analysis. The data are represented as mean ± standard deviation ($n$ = 3). ns, not significant = $p >$ 0.05; * = 0.01 < $p \leq$ 0.05; ** = 0.001 < $p \leq$ 0.01; **** = $p \leq$ 0.0001.

the second row of side valves and shaking the chip, the yellow and red dyes mixed to form an orange color in the coated left channel. In contrast, in the uncoated right channel, the mixture of the red and yellow dyes leaked into the blue resulting a green color before opening the bottom row of the valve. In the right image, after pulling the bottom side valves, the orange dye mixed with blue forming a green color in the coated left channel. Meanwhile, in the uncoated right channel, the green mixture already appeared during the second step. The valves in the middle channel, coated with NeverWet, prevented any leakage or mixing. Higher viscosity fluids, such as RPA reagents, resist flow more than lower viscosity fluids, such as food dye. In our experiments, we observed less leaking for RPA reagents due to their slower flow rates,[35] making the food dye test a more stringent challenge.

Clear visualization of the reactions is critical for accurate result interpretation, as any surface imperfections can scatter light or cause distortions, ultimately reducing the clarity of the output. The vapor smoothing eliminates the layer lines formed during the 3D printing process and results in a glossy finish on the core surface. This process transformed the replicated PDMS surface from translucent to transparent, which improved the visibility of users to observe the status of the chambers. As shown in Figure 2b, evaluated under SEM, vapor smoothing not only improved the visual appearance but also enhanced the performance of the MFAST chip. Figure 2c shows that this process increased the transport efficiency of liquids by reducing the layer lines that could trap fluid during transport. The efficiency of liquid transport was tested by measuring the amount of food dye transferred from the second row of the MFAST chip to the third row. Results demonstrated that the combination of vapor smoothing and NeverWet coating treatment improved the transport efficiency by about 25%. The NeverWet coating, by creating a superhydrophobic surface, reduced liquid adhesion to the valve and repelled fluid trapped in the intricate design of the valves. In this test, food dye was added to the second row of the chip, and the amount of remaining dye was measured after the chip was shaken five times with all valves closed. The results, shown in Figure 2d, revealed that the NeverWet coating reduced leakage by more than 20%, providing significant protection against leaks.

To improve liquid transfer, the water contact angle of the inner MFAST chip chamber was altered. Our simulation, as shown in Figure 3a, illustrates that making the inner surface of the MFAST chip more hydrophilic, by reducing the contact angle with water to 30°, results in a more efficient flow pattern. With that in mind, oxygen plasma treatment was used to decrease the water contact angle of the MFAST chip's inner surface.[36] As shown in Figure 3b, the water contact angle of the inner cavity surface dropped from 106.05 to 39.09° after the plasma treatment. We found that the transportation of the fluid to the subsequent chamber became much easier after the plasma treatment, where only a little tap was required.

The specificity and sensitivity of the RPA-CRISPR assay for the detection of *L. panamensis* were subsequently evaluated. To assess specificity, fluorescence was compared between *L. panamensis* at a concentration of $1 \times 10^6$ parasites/mL and six other *Leishmania* strains, namely *L. braziliensis*, *L. gerbelli*, *L. infantum*, *L. tropica*, *L. donovani*, and *L. venezuelensis*, as well as a non-template control (NTC). The end point fluorescence images of the reactions are shown in Figure 4a. Upon excitation with a blue light transilluminator, the fluorescence differences between *L. panamensis* and the other groups were clearly distinguishable by the naked eye. The normalized fluorescence signal is presented in Figure 4b, indicating that the fluorescence intensity of the six non-target strains and the NTC group was significantly lower than that of *L. panamensis*, demonstrating the high specificity of the RPA-CRISPR assay. To determine the detection limit, different concentrations of *L. panamensis* were used as targets and added to the RPA mixture. Following the RPA reaction, the amplicons were introduced into a premixed CRISPR reaction and incubated at 37 °C for


https://doi.org/10.1021/acssensors.4c03306
ACS Sens. XXXX, XXX, XXX−XXX

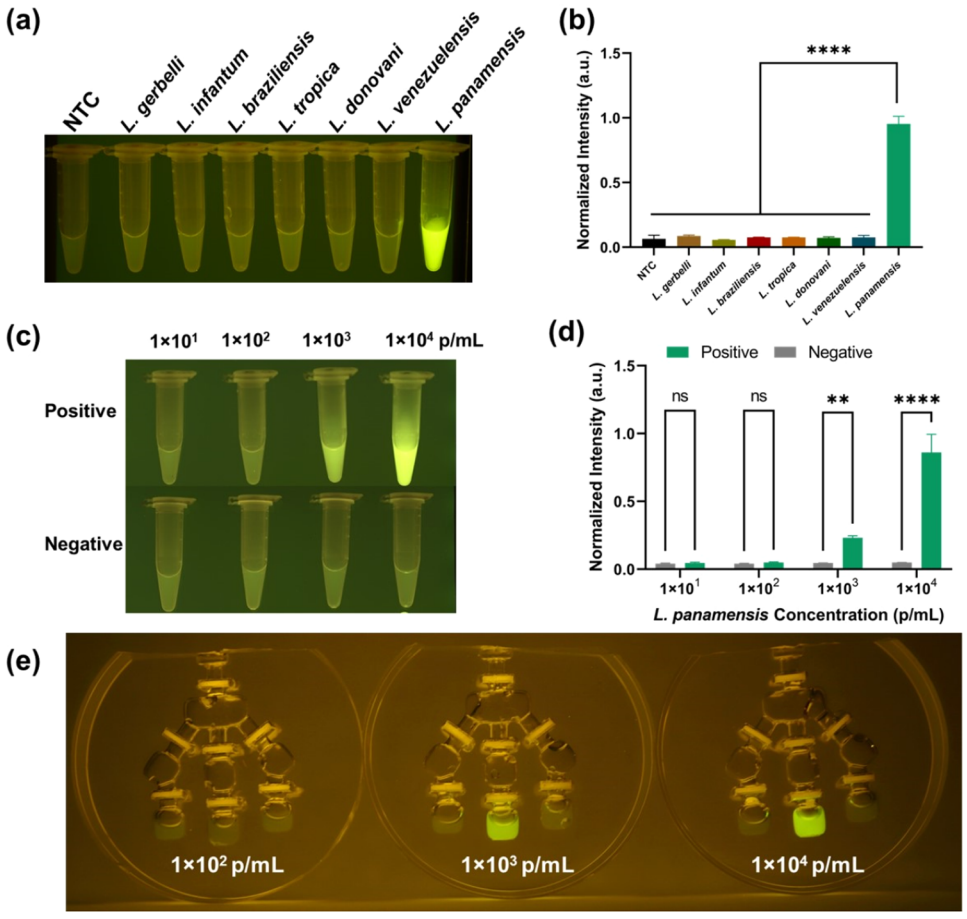



**Figure 4.** (a) End point images of the reactions with $1 \times 10^6$ parasites/mL of different *Leishmania* strains. Fluorescence was excited by a transilluminator (wavelength: 465 nm). (b) Normalized fluorescence signals of the reactions with $1 \times 10^6$ parasites/mL of different *Leishmania* strains. Statistical analyses were performed using one-way ANOVA. (c) End point images of the reactions excited by a transilluminator (excitation wavelength: 465 nm) in response to different *L. panamensis* concentrations ranging from 10 to $1 \times 10^4$ parasites/mL. (d) Normalized fluorescence signals of the reactions with different *L. panamensis* concentrations ranging from 10 to $1 \times 10^4$ parasites/mL. Statistical analyses were performed using two-way ANOVA. (e) End point images of the on-chip reactions excited by a transilluminator (excitation wavelength: 465 nm) in response to different *L. panamensis* concentrations ranging from 100 to $1 \times 10^4$ parasites/mL. "NTC" refers to no template control. The data are represented as mean ± standard deviation ($n$ = 3). ns, not significant = $p > 0.05$; * = $0.01 < p \leq 0.05$; ** = $0.001 < p \leq 0.01$; **** = $p \leq 0.0001$.

30 min. For the negative control groups, either the RPA primers or crRNAs were replaced with nuclease-free water. The end point fluorescence images of the reaction are shown in Figure 4c, with the corresponding normalized fluorescence signals presented in Figure 4d. Distinct fluorescence differences were observed at concentrations of $1 \times 10^3$ parasites/mL (corresponding to DNA from 5 parasites) and $1 \times 10^4$ parasites/mL (corresponding to DNA from 50 parasites). However, no significant fluorescence difference between positive and negative groups was detected at a concentration of $1 \times 10^2$ parasites/mL (corresponding to DNA from 0.5 parasite) or lower. The on-chip detection results are presented in Figure. 4e. The left channel represents the negative group without RPA primers, while the right channel represents the positive group without crRNAs. Compared to the negative groups, the positive group exhibited a significantly stronger fluorescence signal at a concentration of $1 \times 10^3$ parasites/mL (as few as 5 parasites per reaction), demonstrating consistency with the off-chip results.

Since the chip was designed with multiple channels, it can be applied for duplex detection by loading two sets of RPA primers and crRNAs targeting different *Leishmania* species. One channel was used for the detection of all seven *Leishmania* species, while another channel was specific for *L. panamensis*, which is associated with mucocutaneous diseases. The third channel served as a negative control without RPA primers. Among the seven species, *L. braziliensis* was used as the sole target, with the CRISPR and RPA reagents for detecting all seven species loaded into the right channel, while the left two channels served as negative controls. The results presented in Figure 5a (left) indicate that the positive group generated noticeably stronger fluorescence compared with the negative controls, demonstrating effective detection of the target without cross-contamination and false-positive results. When a 1:1 mixture of *L. panamensis* and *L. braziliensis* was analyzed, the RPA and CRISPR reagents specific to *L. panamensis* were loaded into the left channel of the MFAST chip. As shown in Figure 5a (right), both the left and right channels displayed strong green fluorescence, whereas the middle negative group did not, thereby confirming the successful duplex detection of both species. The quantitative normalized fluorescence intensity in Figure 5b further supports these findings, showing that the *Leishmania* groups exhibited a considerably higher fluorescence intensity compared to the negative control.

To enhance the storage stability,[37] ease of transportation,[38] and overall usability of the MFAST chip, the reagents were


https://doi.org/10.1021/acssensors.4c03306
ACS Sens. XXXX, XXX, XXX−XXX

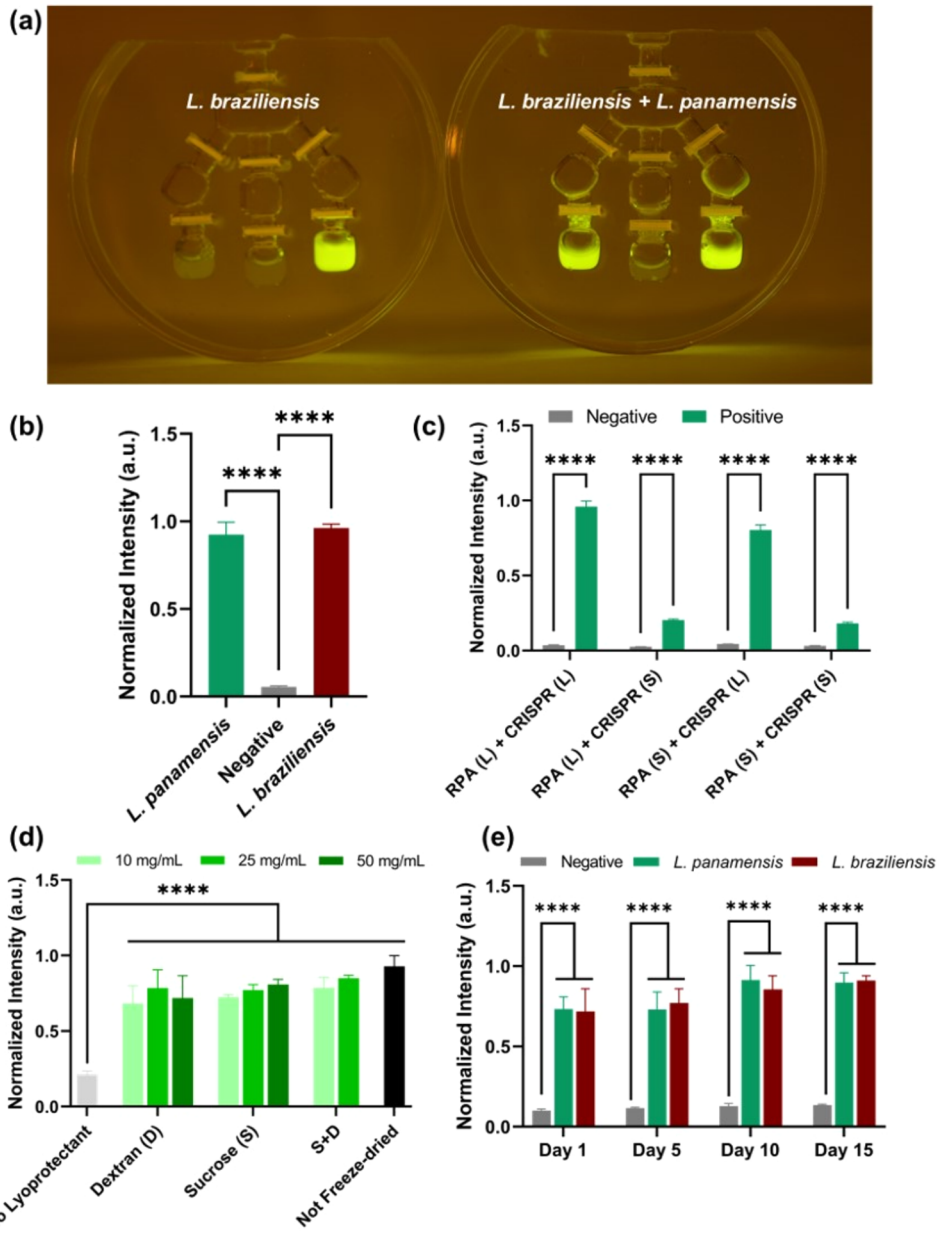



**Figure 5.** (a) End point images of the on-chip reaction with $1 \times 10^6$ parasites/mL of *L. braziliensis* (left) and a 1:1 mixture of *L. panamensis* and *L. braziliensis*. In the left image, the two left channels represent negative controls. In the right image, the middle channel serves as a negative control. Fluorescence was excited by a transilluminator (wavelength: 465 nm). (b) Normalized fluorescence signals from the reactions with $1 \times 10^6$ parasites/mL of a 1:1 mixture of *L. panamensis* and *L. braziliensis*. Statistical analyses were performed using one-way ANOVA. (c) Impact of lyophilization on the performance of RPA and CRISPR reactions. (d) Performance of lyophilized reactions supplemented with dextran and/or sucrose at concentrations of 10, 25, and 50 mg/mL. (e) Stability test of lyophilized reactions stored at 4 °C. Statistical analyses for lyophilization results were performed using two-way ANOVA. The data are represented as mean ± standard deviation ($n = 3$). ns, not significant = $p > 0.05$; * = $0.01 < p \leq 0.05$; ** = $0.001 < p \leq 0.01$; **** = $p \leq 0.0001$.

subjected to lyophilization. This process involves initially freezing the reagents, followed by the sublimation of water during the primary drying phase. Secondary drying is then conducted to eliminate residual moisture and achieve the target final moisture content.[39] The RPA and CRISPR reagents were lyophilized independently, and their performances were subsequently evaluated and compared. The enzyme pellet in the RPA kit, which was originally supplied in lyophilized form, was added after the RPA reagents underwent the freeze-drying process. The input target was 1:1 mixture of *L. panamensis* and *L. braziliensis* with the concentration of $1 \times 10^6$ parasites/mL. The results, as shown in Figure 5c, demonstrate that the fluorescence intensity generated by the lyophilized solid form (S) was significantly lower than that of the liquid reagents (L), indicating a reduction in assay performance. To protect Cas12a during freeze-drying, stabilizing agents like dextran and/or sucrose were added to maintain its structure and functionality.[40] As shown in Figure 5d, we found that the activity of reactions increased with sucrose concentration and dextran exhibited a concentration optimum of 25 mg/mL in the final reaction. Combining 25 mg/mL each of sucrose and dextran exhibited approximately 85% recovery of the prelyophilization signal. Additionally, we assessed the stability of the lyophilized reagents stored at 4 °C. As depicted in Figure 5e, the


https://doi.org/10.1021/acssensors.4c03306
ACS Sens. XXXX, XXX, XXX−XXX

lyophilized reagents remained functional and stable for up to 15 days.

The freeze-drying process negatively affected the efficiency of both RPA and CRISPR reactions, with a more pronounced reduction observed for CRISPR, likely due to the loss of Cas12a activity during lyophilization. This loss can be attributed to stresses induced during the lyophilization process, including cold denaturation, exposure to ice−water interfaces, and freeze concentration, which can lead to protein unfolding or aggregation. During the drying phases, the removal of water also affects its structural integrity, potentially causing irreversible denaturation.[41] Excipients such as dextran and sucrose form hydrogen bonds with specific sites on the protein surface, effectively replacing the thermodynamic stabilization role of water that is lost during drying. This process increases the free energy of protein unfolding, thereby preventing denaturation and preserving the native structure, ultimately enhancing storage stability.[42] A recent study demonstrated that lyophilized reagents stored at room temperature retained approximately 75% of their activity after two months.[40] This suggests that short-term storage and transport at room temperature may be feasible.

Compared to previous FAST chips,[33] the chip design has changed from one column to three columns for duplex detection. The valve design was changed from a carbon fiber rod to a 3D-printed flat valve with NeverWet coating to enhance the sealing between the chambers so that the FAST chip no longer needed to be cut into two pieces. The MFAST chip chose ABS rather than the poly(vinyl alcohol) (PVA) used for the FAST chip. Due to its material properties, ABS material used as a sacrificial core has better printability, cheaper material cost, and requires less than half of the time to produce compared to the original FAST chip.[43,44] Our new process also improves the visibility of the chip by employing an acetone vapor smoothing technique, which removes the layer lines left by 3D printing. This method effectively polishes away surface imperfections and results in a clearer final product.[45−48] Plasma treatment of the chamber was added to improve the fluid flow between the chambers as it introduced hydrophilic oxygen-containing groups to the treated surfaces.[49] Overall, the vapor smoothing, NeverWet coating, and plasma treatment were to improve the usability and reliability of the MFAST chip, which is an important step toward real-world applications.

This multi-channel setup enables both positive and negative results to be observed simultaneously on a single chip by simply adding the sample into the reagent-preloaded system, streamlining the detection process of ML-causing species such as *L. panamensis* and minimizing the risk of false positives. By integration of both positive and negative reactions into a closed system, the chip significantly reduces contamination risks, simplifies handling, and enhances its suitability for rapid POC diagnostics. Moreover, the duplex detection design allows for the simultaneous detection of different *Leishmania* species within a single run, increasing throughput and shortening assay time compared to sequential testing. This not only conserves reagents by running multiple assays on the same chip, lowering the overall costs, but also improves result reliability through integrated negative controls for real-time comparison, further reducing the chances of false positives.

Other detection and quantification methods of the parasitic such as microscopy,[50] Raman spectrometry,[51] and quartz crystal microbalance[52] would require trained technicians and expensive equipment. On the other hand, the MFAST device only requires a heating device and a UV flashlight and does not require a lab environment to perform the test. Its lightweight, compact design also makes it ideal for POC use while being advantageous for packing and shipping, conserving space, and helping to keep the overall diagnostic cost low. Compared to the traditional optical-based technique, the user can quickly determine the result based on the fluorescence signal without the need for a detection device or training.[53,54]

Using 3D printing to produce sacrificial molds offers designers greater flexibility for creating intricate or unconventional geometries, as well as faster turnaround times for small test batches.[55,56] This approach supports rapid prototyping by enabling quick design iterations and on-demand manufacturing. The 3D-printed coarse surface could be compensated with the vapor smoothing process, even though the dimension accuracy would be slightly compromised, because the surface material would be melted by the acetone vapor. In the future, it is possible to switch the 3D-printed sacrificial core with an injection-molded sacrificial core, which would dramatically decrease the production time of the core as the injection molding could produce the same part within seconds and the 3D printing takes minutes. The injection molding process could also control the surface finish by altering the mold, and therefore eliminate the need for a vapor smoothing process while maintaining the dimension accuracy.[57]

By alteration of the water contact angle of the inner surface of the MFAST chamber with plasma treatment, the flow property was changed. In the future, the inner surface would include microstructures, such as the super hydrophilic honeycomb structure,[58] to achieve long-lasting hydrophilicity to give the FAST chip a longer shelf life. During the testing of the chip, it was observed that the distribution of the liquid when transporting from the top row of the chamber to the middle row was not even, where the middle column would have more liquid than the other two columns. In future work, the diameter of the channel could be changed with the help of simulation to produce an even distribution of the liquid across all of the chambers and allow it for more than three columns.

## CONCLUSIONS

We developed an all-in-one multi-channel funnel adapted sensing tube (MFAST) chip using sacrificial molding for in vitro detection of species that cause mucosal leishmaniasis such as *L. panamensis*. Several surface treatments were applied to enhance its performance. By applying vapor smoothing and NeverWet coating treatments, transport efficiency improved by roughly 25%, while the leaking rate decreased by over 20%. Additionally, plasma treatment was performed on the inner surfaces of the MFAST chip to increase hydrophilicity, facilitating smoother liquid flow, as demonstrated in simulation results. For detection, we employed the RPA-CRISPR/Cas12a assay, which showed high specificity for *L. panamensis* compared to other *Leishmania* strains, along with a sensitivity of 1000 parasites/mL (as few as 5 parasites per reaction). To expand its diagnostic capabilities, the multi-channel design of MFAST enabled duplex detection by incorporating distinct primers and crRNAs in separate channels. This successfully achieved the simultaneous detection of *L. braziliensis* and *L. panamensis* without cross-contamination. Furthermore, we tested the stability of lyophilized reagents preloaded in the chip. With excipients of 25 mg/mL of sucrose and dextran, the lyophilized reagents remained functional and stable for up to


https://doi.org/10.1021/acssensors.4c03306
ACS Sens. XXXX, XXX, XXX−XXX

15 days. The MFAST chip demonstrates a promising platform for leishmaniasis diagnosis, offering potential for multiplexing and reagent stability in field settings.

## EXPERIMENTAL SECTION

**Fabrication of MFAST Chip.** The 3D model of the MFAST chip core was designed by using SolidWorks. It was fabricated using a fused deposition modeling X1 Carbon 3D printer (Bambu Lab) with PolyLite ABS (Polymaker) material. The printed core was then suspended in the vapor smoothing chamber with a copper wire for 1.5 min to remove the layer lines. The vapor smoothing chamber consists of a tall glass jar with approximately 1 cm of 100% acetone covering the bottom and was heated at 90 °C. During this period, the vapored acetone would dissolve the surface of the printed ABS core, therefore removing the layer line and creating a glossy finish. The hooks, designed for hanging by the wire, were snipped off after the smoothing process. It was then glued on a 60 × 15 mm Petri dish with super glue (Loctite). The 10:1 ratio mixture of the Polydimethylsiloxane (SYLGARD 184 Silicone Elastomer Kit base) and curing agent was poured into a Petri dish and filled to the top. It was then placed at room temperature for 2 days to degas before being placed into an oven at 70 °C for 4 h. After curing, the MFAST chip was submerged with acetone in an ultrasonic cleaner until the ABS core was fully dissolved. The valves of the MFAST chip were 3D-printed using an UltraCraft Reflex 3D Printer combo (HeyGears) with UltraPrint-Modeling PAT10 Transparent Resin (HeyGears). Then, the surface of the valve was coated with NeverWet (Rust-Oleum, No. 274232). The valves were left to dry for 30 min in between the two coating steps. Both steps were applied from approximately 20 cm away and then air-dried at room temperature overnight before use.

**Surface Treatment and Quantification.** The transport efficiency of the chip was measured by adding 100 μL of food dye into the chambers in the second row and then extracting the food dye from the third row after it had been transported and repeated 6 times. The weight of the food dye was measured by using an electronic balance. The leak test was performed by adding 100 μL of food dye into the second row, closing all the valves, and then shaking it 5 times by hand. Then, the liquid remaining in the second row was extracted and measured. The water contact angle of the inner chamber was measured by creating a large flat cavity surface using the same process as that for the MFAST chip with ABS sacrificial molding. It was then cut into a size for the water contact angle testing. The plasma treatment of the MFAST chip was performed by placing it into an oxygen plasma chamber for 10 min with 100 W RF power, 20 sccm $O_2$, and 0.6 mbar pressure.

**Two-Phase Flow Simulation.** The simulation investigates a two-phase flow involving water as the continuous phase and air as the dispersed phase using COMSOL Multiphysics. The primary objective is to model the interaction between the dispersed air phase and the continuous water phase in controlled geometry. The Laminar Flow interface uses the Navier−Stokes equation for incompressible fluid flow, ensuring that the velocity and pressure fields of the continuous water phase are accurately simulated. The Phase Transport interface models the behavior of the dispersed air phase, starting from a closed valve configuration filled with air and transitioning to an open valve, allowing water to flow. Boundary conditions include an inlet velocity defined by a step function, allowing a gradual increase in velocity from 0 to 0.01 m/s to simulate valve opening. The initial conditions set the water as uniformly distributed with air present at a volume fraction of 0.8, representing the initial state with closed valves. The simulation explores different contact angles (30, 100, and 150°) to observe changes in the volume fraction and velocity fields.

**Parasite Culture and Lysis.** The following *Leishmania* species were purchased from BEI Resources: *L. panamensis*, strain PSC-1 (MHOM/PA/94/PSC 1), NR-50162; *L. braziliensis*, strain HOM/BR/75/M2903, NR 50608; *L. gerbelli*, strain RHO/CN/62/20, NR-50601; *L. infantum*, strain HOM/CN/93/KXG-LIU, NR 50605; *L. tropica*, strain HOM/TR/99/EP41, NR-51828; *L. donovani*, strain HOM/IN/83/AG83, NR-50602; *L. venezuelensis*, strain MHOM/VE/80/H-16, NR-29184. The parasites were cultivated in tissue culture by inoculating thawed samples into T-25 flasks containing Modified M199 medium (Gibco, ref: 12350−039) supplemented with 10% heat-inactivated fetal bovine serum (Neuromonics, Cat. No. FBS006) and 10 μg/mL hemin chloride (Millipore Sigma, ref: 3741−5GM) at 25 °C, and subsequently expanded into T-182 flasks. Parasite density was determined using a hemocytometer and adjusted to $5 \times 10^6$ parasites/mL, followed by pelleting at 2000 × g and washing with 1× PBS. Next, 1 mL of 0.1% Triton X-100 in PBS was added, and the mixture was incubated at 56 °C for 10 min.

**RPA Amplification and CRISPR-Cas12a Detection.** The TwistAmp Basic kit was obtained from TwistDx Ltd. NEBuffer r2.1 was purchased from New England Biolabs. The RPA primers, fluorophore-quencher (F-Q) probe, crRNA, and AsCas12a (Alt-R A.s. Cas12a Ultra), were purchased from Integrated DNA Technologies, with detailed information about the synthetic oligonucleotides provided in Table S1. The DNA sequences of different *Leishmania* species were aligned using clustalW and Bioedit, and the RPA primer sets were designed using the Primer 3 program. The crRNAs were designed using CRISPOR.

The target mixture was prepared by combining 5 μL of target with 21.25 μL of nuclease-free water and 3.75 μL of magnesium acetate (280 mM). To prepare RPA mixture, 4.8 μL of each RPA primer (10 μM) was combined with 59 μL of primer-free rehydration buffer, and the TwistAmp Basic reaction pellet was dissolved in the mixture. For the CRISPR mixture, 7.5 μL of crRNA (1 μM) was mixed with 6 μL of Cas12a (1 μM), and the complex was then equilibrated at room temperature for 10 min. Subsequently, 12 μL of NEBuffer r2.1 (10×) and 1 μL of the ssDNA probe (100 μM) were added to complete the CRISPR mixture.

The target mixture was added to the RPA mixture, where the magnesium acetate contained in the target mixture initiated the RPA reaction. The reaction was incubated at 37 °C for 20 min. Following this, the mixture was added to the preassembled CRISPR mixture and incubated at 37 °C for 30 min.

***Leishmania* Detection with MFAST.** The CRISPR mixture was pipetted into the bottom chamber, and valves were inserted into the bottom gaps to seal the CRISPR reagents. Subsequently, the RPA mixture was introduced into the second chamber, and the valves were inserted into the corresponding gaps to seal the RPA reagents. The target mixture was then introduced into the top chamber and sealed with valves. For negative controls, either the RPA primers or the crRNAs were replaced with nuclease-free water. To initiate the reaction, the second row of valves was pulled to allow the target mixture to flow into the RPA chamber. The MFAST chip was then incubated on a heating pad at 37 °C for 20 min. Following this incubation, the bottom valves were pulled to allow the mixture to flow into the CRISPR chamber, which was incubated at 37 °C for an additional 30 min. A blue light transilluminator (SmartBlue, Part No: NEB-E4100, excitation wavelength of 465 nm) was subsequently used to excite the mixture for naked eye observation. Finally, 20 μL of nuclease-free water was added to 5 μL of the mixture, and the resulting solution was characterized by using an Agilent BioTek Cytation 5 imaging reader.

**Lyophilization.** For the off-chip assay, given that the RPA enzymatic pellets were provided in a lyophilized form, the lyoprotectant dextran or sucrose was incorporated into the CRISPR reaction prior to transferring the mixture to PCR strip tubes, each with a small hole punctured in the cap. When a 384-well plate was used, a PCR sealing film (Thermo Fisher Scientific) was applied over the wells, with a small hole punctured in each well. The RPA and CRISPR reactions were subsequently prefrozen and freeze-dried in a freeze-dryer (Harvest Right, Model No: HRFD-SML-BK) overnight. For the on-chip lyophilization, following the loading of reagents into the respective chambers, the chip was laid flat with the valves slightly open to leave a gap, and then prefrozen and freeze-dried in a freeze-dryer overnight.


https://doi.org/10.1021/acssensors.4c03306
ACS Sens. XXXX, XXX, XXX−XXX

## ■ ASSOCIATED CONTENT

### Supporting Information

The Supporting Information is available free of charge at https://pubs.acs.org/doi/10.1021/acssensors.4c03306.

Oligos sequence used in this study (Table S1) (PDF)

## ■ AUTHOR INFORMATION


### Corresponding Authors

**Stephen J. Dollery** − *Biological Mimetics, Inc., Frederick, Maryland 21702, United States*

**Ke Du** − *Department of Chemical and Environmental Engineering, University of California, Riverside, Riverside, California 92507, United States;* orcid.org/0000-0002-6837-0927

### Authors

**Ruonan Peng** − *Department of Chemical and Environmental Engineering, University of California, Riverside, Riverside, California 92507, United States*

**FNU Yuqing** − *Department of Chemical and Environmental Engineering and Department of Mechanical Engineering, University of California, Riverside, Riverside, California 92507, United States*

**Taralyn J. Wiggins** − *Biological Mimetics, Inc., Frederick, Maryland 21702, United States*

**Negin Bahadori** − *Department of Chemical and Environmental Engineering, University of California, Riverside, Riverside, California 92507, United States; Mechanical Engineering, College of Engineering and Science, Louisiana Tech University, Ruston, Louisiana 71272, United States*

**Joshua S. Rogers** − *Charlie Dunlop School of Biological Sciences, University in Irvine, California, Irvine, California 92697, United States*

**Jacob Waitkus** − *Department of Chemical and Environmental Engineering, University of California, Riverside, Riverside, California 92507, United States*

**Yun Chen** − *Mechanical Engineering, College of Engineering and Science, Louisiana Tech University, Ruston, Louisiana 71272, United States; Department of Mechanical Engineering, California State Polytechnic University, Pomona, California 91768, United States*

**Gregory J. Tobin** − *Biological Mimetics, Inc., Frederick, Maryland 21702, United States*

Complete contact information is available at: https://pubs.acs.org/10.1021/acssensors.4c03306


### Author Contributions

[▽]R.P. and F.Y. these authors contributed equally to this work. R.P., F.Y., G.J.T., S.J.D., and K.D. designed the experiments. R.P., F.Y., T.J.W., N.B., J.S.R., and J.W. performed the experiments. R.P. and F.Y. wrote the manuscript. All authors commented on the manuscript.

### Notes

The authors declare no competing financial interest.

A preprint of this article was posted on bioRxiv. {Ruonan Peng, Fnu Yuqing, Taralyn J. Wiggins, Negin Bahadori, Stephen J. Dollery, Jacob Waitkus, Joshua S. Rogers, Yun Chen, Gregory J. Tobin, Ke Du, bioRxiv 2024.10.19.619249} DOI: "10.1101/2024.10.19.619249" (accessed − 02/25/2025)

## ■ ACKNOWLEDGMENTS

This project was supported by NIH NIAID (R43AI179513-01 and 75N93023C00056-0-9999-1), University of California OASIS Internal Grant, and NSF RII Track-4 (2327429).

## ■ REFERENCES


(1) Savoia, D. Recent Updates and Perspectives on Leishmaniasis. *J. Infect. Dev. Countries* **2015**, *9* (06), 588−596.

(2) Wiggins, T. J.; Peng, R.; Bushnell, R. V.; Tobin, J. K.; MacLeod, D. A.; Du, K.; Tobin, G. J.; Dollery, S. J. Instrument-Free Point-of-Care Diagnostic for *Leishmania* Parasites. *Diagnostics* **2024**, *14* (23), 2744.

(3) Steverding, D. The History of Leishmaniasis. *Parasites Vectors* **2017**, *10*, No. 82.

(4) Torres-Guerrero, E.; Quintanilla-Cedillo, M. R.; Ruiz-Esmenjaud, J.; Arenas, R. Leishmaniasis: A Review. *F1000Research* **2017**, *6*, No. 750.

(5) Welearegay, T. G.; Diouani, M. F.; Österlund, L.; Ionescu, F.; Belgacem, K.; Smadhi, H.; Khaled, S.; Kidar, A.; Laouini, D.; Cindemir, U.; et al. Ligand-Capped Ultrapure Metal Nanoparticle Sensors for the Detection of Cutaneous Leishmaniasis Disease in Exhaled Breath. *ACS Sens.* **2018**, *3* (12), 2532−2540.

(6) Gow, I.; Smith, N. C.; Stark, D.; Ellis, J. Laboratory Diagnostics for Human Leishmania Infections: A Polymerase Chain Reaction-Focussed Review of Detection and Identification Methods. *Parasites Vectors* **2022**, *15* (1), No. 412.

(7) Malafaia, G. Protein-Energy Malnutrition as a Risk Factor for Visceral Leishmaniasis: A Review. *Parasite Immunol.* **2009**, *31* (10), 587−596.

(8) Alvar, J.; Yactayo, S.; Bern, C. Leishmaniasis and Poverty. *Trends Parasitol.* **2006**, *22* (12), 552−557.

(9) Costa-da-Silva, A. C.; Nascimento, D.; de, O.; Ferreira, J. R.; Guimarães-Pinto, K.; Freire-de-Lima, L.; Morrot, A.; Decote-Ricardo, D.; Filardy, A. A.; Freire-de-Lima, C. G. Immune Responses in Leishmaniasis: An Overview. *Trop. Med. Infect. Dis.* **2022**, *7* (4), No. 54.

(10) Okwor, I.; Uzonna, J. Social and Economic Burden of Human Leishmaniasis. *Am. J. Trop. Med. Hyg.* **2016**, *94* (3), No. 489.

(11) Mann, S.; Frasca, K.; Scherrer, S.; Henao-Martínez, A. F.; Newman, S.; Ramanan, P.; Suarez, J. A. A Review of Leishmaniasis: Current Knowledge and Future Directions. *Curr. Trop. Med. Rep.* **2021**, *8*, 121−132.

(12) El Hajj, R.; El Hajj, H.; Khalifeh, I. Fatal Visceral Leishmaniasis Caused by *Leishmania* Infantum, Lebanon. *Emerging Infect. Dis.* **2018**, *24* (5), No. 906.

(13) Carvalho, J. de P.; Silva, S. N.; Freire, M. L.; Alves, L. L.; Souza, C. S. A. de.; Cota, G. The Cure Rate after Different Treatments for Mucosal Leishmaniasis in the Americas: A Systematic Review. *PLoS Neglected Trop. Dis.* **2022**, *16* (11), No. e0010931.

(14) Casalle, N.; de Barros Pinto Grifoni, L.; Bosco Mendes, A. C.; Delort, S.; Massucato, E. M. S. Mucocutaneous Leishmaniasis with Rare Manifestation in the Nasal Mucosa and Cartilage Bone Septal. *Case Rep. Infect. Dis.* **2020**, *2020* (1), No. 8876020.

(15) Fischer, T.; Fischer, M.; Schliemann, S.; Elsner, P. Treatment of Mucocutaneous Leishmaniasis−A Systematic Review. *J. Dtsch. Dermatol. Ges.* **2024**, *22* (6), 763−773, DOI: 10.1111/ddg.15424.

(16) Burza, S.; Croft, S.; Marleen, B. Leishmaniasis *Lancet* 2018; Vol. *15* 392, p 10151.

(17) Peng, R.; Chen, X.; Xu, F.; Hailstone, R.; Men, Y.; Du, K. Pneumatic Nano-Sieve for CRISPR-Based Detection of Drug-Resistant Bacteria. *Nanoscale Horiz.* **2023**, *8* (12), 1677−1685.

(18) Singh, O. P.; Sundar, S. Developments in Diagnosis of Visceral Leishmaniasis in the Elimination Era. *J. Parasitol. Res.* **2015**, *2015* (1), No. 239469.

(19) de Vries, H. J.; Reedijk, S. H.; Schallig, H. D. Cutaneous Leishmaniasis: Recent Developments in Diagnosis and Management. *Am. J. Clin. Dermatol.* **2015**, *16*, 99−109.

(20) de Vries, H. J.; Schallig, H. D. Cutaneous Leishmaniasis: A 2022 Updated Narrative Review into Diagnosis and Management Developments. *Am. J. Clin. Dermatol.* **2022**, *23* (6), 823−840.
(21) Gomes, C. M.; Mazin, S. C.; Santos, E. R. dos.; Cesetti, M. V.; Bächtold, G. A. B.; Cordeiro, J. H. de F.; Theodoro, F. C. E. T.; Damasco, F. dos S.; Carranza, S. A. V.; Santos, A. de O.; et al. Accuracy of Mucocutaneous Leishmaniasis Diagnosis Using Polymerase Chain Reaction: Systematic Literature Review and Meta-Analysis. *Mem. Inst. Oswaldo Cruz* **2015**, *110* (2), 157−165.
(22) He, J.; Peng, R.; Yuqing, H.; Karim, R.; Chen, J.; Lu, G.; Du, K. Superhydrophobic Rotation-Chip for Computer-Vision Identification of Drug-Resistant Bacteria. *ACS Appl. Mater. Interfaces* **2023**, *15*, 27732−27741.
(23) Lou, J.; Wang, B.; Li, J.; Ni, P.; Jin, Y.; Chen, S.; Xi, Y.; Zhang, R.; Duan, G. The CRISPR-Cas System as a Tool for Diagnosing and Treating Infectious Diseases. *Mol. Biol. Rep.* **2022**, *49* (12), 11301−11311.
(24) Paul, B.; Montoya, G. CRISPR-Cas12a: Functional Overview and Applications. *Biomed. J.* **2020**, *43* (1), 8−17.
(25) Xiong, Y.; Zhang, J.; Yang, Z.; Mou, Q.; Ma, Y.; Xiong, Y.; Lu, Y. Functional DNA Regulated CRISPR-Cas12a Sensors for Point-of-Care Diagnostics of Non-Nucleic-Acid Targets. *J. Am. Chem. Soc.* **2020**, *142* (1), 207−213.
(26) Kasputis, T.; He, Y.; Ci, Q.; Chen, J. On-Site Fluorescent Detection of Sepsis-Inducing Bacteria Using a Graphene-Oxide CRISPR-Cas12a (GO-CRISPR) System. *Anal. Chem.* **2024**, *96* (6), 2676−2683.
(27) Rananaware, S. R.; Vesco, E. K.; Shoemaker, G. M.; Anekar, S. S.; Sandoval, L. S. W.; Meister, K. S.; Macaluso, N. C.; Nguyen, L. T.; Jain, P. K. Programmable RNA Detection with CRISPR-Cas12a. *Nat. Commun.* **2023**, *14* (1), No. 5409.
(28) Zarei, M. Advances in Point-of-Care Technologies for Molecular Diagnostics. *Biosens. Bioelectron.* **2017**, *98*, 494−506.
(29) Lobato, I. M.; O'Sullivan, C. K. Recombinase Polymerase Amplification: Basics, Applications and Recent Advances. *TrAC, Trends Anal. Chem.* **2018**, *98*, 19−35.
(30) Jiang, Y.; Hu, M.; Liu, A.-A.; Lin, Y.; Liu, L.; Yu, B.; Zhou, X.; Pang, D.-W. Detection of SARS-CoV-2 by CRISPR/Cas12a-Enhanced Colorimetry. *ACS Sens.* **2021**, *6* (3), 1086−1093.
(31) Daher, R. K.; Stewart, G.; Boissinot, M.; Bergeron, M. G. Recombinase Polymerase Amplification for Diagnostic Applications. *Clin. Chem.* **2016**, *62* (7), 947−958.
(32) Yin, K.; Ding, X.; Li, Z.; Zhao, H.; Cooper, K.; Liu, C. Dynamic Aqueous Multiphase Reaction System for One-Pot CRISPR-Cas12a-Based Ultrasensitive and Quantitative Molecular Diagnosis. *Anal. Chem.* **2020**, *92* (12), 8561−8568.
(33) Bao, M.; Zhang, S.; Ten Pas, C.; Dollery, S. J.; Bushnell, R. V.; Yuqing, F.; Liu, R.; Lu, G.; Tobin, G. J.; Du, K. Computer Vision Enabled Funnel Adapted Sensing Tube (FAST) for Power-Free and Pipette-Free Nucleic Acid Detection. *Lab Chip* **2022**, *22* (24), 4849−4859.
(34) Verma, S.; Kumar, R.; Katara, G. K.; Singh, L. C.; Negi, N. S.; Ramesh, V.; Salotra, P. Quantification of Parasite Load in Clinical Samples of Leishmaniasis Patients: IL-10 Level Correlates with Parasite Load in Visceral Leishmaniasis. *PloS one* **2010**, *5* (4), No. e10107.
(35) Jiang, Q.; Xu, P.; Xu, J.; Hou, M.; Liu, Q.; Dai, B. Preparation and Evaluation of Composite Hydrogel for Reducing the Leakage Rate of Lost Circulation. *Polymers* **2023**, *15* (21), 4218.
(36) Vickers, J. A.; Caulum, M. M.; Henry, C. S. Generation of Hydrophilic Poly (Dimethylsiloxane) for High-Performance Microchip Electrophoresis. *Anal. Chem.* **2006**, *78* (21), 7446−7452.
(37) Luo, W.-C.; Beringhs, A. O.; Kim, R.; Zhang, W.; Patel, S. M.; Bogner, R. H.; Lu, X. Impact of Formulation on the Quality and Stability of Freeze-Dried Nanoparticles. *Eur. J. Pharm. Biopharm.* **2021**, *169*, 256−267.
(38) Bensch, H. M.; Tolf, C.; Waldenström, J.; Lundin, D.; Zöttl, M. Freeze-Drying Can Replace Cold-Chains for Transport and Storage of Fecal Microbiome Samples. *PeerJ.* **2022**, *10*, No. e13095.
(39) Roy, I.; Gupta, M. N. Freeze-Drying of Proteins: Some Emerging Concerns. *Biotechnol. Appl. Biochem.* **2004**, *39* (2), 165−177.
(40) Rybnicky, G. A.; Dixon, R. A.; Kuhn, R. M.; Karim, A. S.; Jewett, M. C. Development of a Freeze-Dried CRISPR-Cas12 Sensor for Detecting Wolbachia in the Secondary Science Classroom. *ACS Synth. Biol.* **2022**, *11* (2), 835−842.
(41) Mutukuri, T. T.; Wilson, N. E.; Taylor, L. S.; Topp, E. M.; Zhou, Q. T. Effects of Drying Method and Excipient on the Structure and Physical Stability of Protein Solids: Freeze Drying vs. Spray Freeze Drying. *Int. J. Pharm.* **2021**, *594*, No. 120169.
(42) Chang, L. L.; Shepherd, D.; Sun, J.; Ouellette, D.; Grant, K. L.; Tang, X. C.; Pikal, M. J. Mechanism of Protein Stabilization by Sugars during Freeze-Drying and Storage: Native Structure Preservation, Specific Interaction, and/or Immobilization in a Glassy Matrix? *J. Pharm. Sci.* **2005**, *94* (7), 1427−1444.
(43) Chen, P.; Chiang, C.-H.; Morbioli, G. G.; Speller, N. C.; Stockton, A. M. A Practical Guide to Rapid-Prototyping of PDMS-Based Microfluidic Devices: A Tutorial. *Anal. Chim. Acta* **2020**, *1135*, 150−174.
(44) Hwang, Y.; Candler, R. N. Non-Planar PDMS Microfluidic Channels and Actuators: A Review. *Lab Chip* **2017**, *17* (23), 3948−3959.
(45) Chen, P.-C.; Chou, C. C.; Chiang, C. H. Systematically Studying Dissolution Process of 3D Printed Acrylonitrile Butadiene Styrene (ABS) Mold for Creation of Complex and Fully Transparent Polydimethylsiloxane (PDMS) Fluidic Devices. *BioChip J.* **2021**, *15*, 144−151.
(46) Maidin, S.; Rajendran, T. K.; Shahrum, M. A.; Norddin, M. F. M.; Ismail, S.; Kamarulnizam, M. Investigation on Surface Roughness of Ultrasonic Assisted Vapour Smoothing of Acrylonitrile Butadiene Styrene Printed Sample. *Eng. Res. Express* **2024**, *6* (2), No. 025402.
(47) Demircali, A. A.; Yilmaz, D.; Yilmaz, A.; Keskin, O.; Keshavarz, M.; Uvet, H. Enhancing Mechanical Properties and Surface Quality of FDM-Printed ABS: A Comprehensive Study on Cold Acetone Vapor Treatment. *Int. J. Adv. Des. Manuf. Technol.* **2024**, *130* (7), 4027−4039.
(48) Yadav, A.; Prakash, B. P.; Dileep, K. S.; Rao, S. A.; Kumar, G. V. An Experimental Examination on Surface Finish of FDM 3D Printed Parts. *Mater. Today: Proc.* **2024**, *115*, 148−155.
(49) Neves, L. B.; Afonso, I. S.; Nobrega, G.; Barbosa, L. G.; Lima, R. A.; Ribeiro, J. E. A Review of Methods to Modify the PDMS Surface Wettability and Their Applications. *Micromachines* **2024**, *15* (6), No. 670.
(50) Mudanyali, O.; Oztoprak, C.; Tseng, D.; Erlinger, A.; Ozcan, A. Detection of Waterborne Parasites Using Field-Portable and Cost-Effective Lensfree Microscopy. *Lab Chip* **2010**, *10* (18), 2419−2423.
(51) Rule, K. L.; Vikesland, P. J. Surface-Enhanced Resonance Raman Spectroscopy for the Rapid Detection of Cryptosporidium Parvum and Giardia Lamblia. *Environ. Sci. Technol.* **2009**, *43* (4), 1147−1152.
(52) Poitras, C.; Fatisson, J.; Tufenkji, N. Real-Time Microgravimetric Quantification of Cryptosporidium Parvum in the Presence of Potential Interferents. *Water Res.* **2009**, *43* (10), 2631−2638.
(53) Bridle, H.; Kersaudy-Kerhoas, M.; Miller, B.; Gavriilidou, D.; Katzer, F.; Innes, E. A.; Desmulliez, M. P. Detection of Cryptosporidium in Miniaturised Fluidic Devices. *Water Res.* **2012**, *46* (6), 1641−1661.
(54) Sánchez-Ovejero, C.; Benito-Lopez, F.; Díez, P.; Casulli, A.; Siles-Lucas, M.; Fuentes, M.; Manzano-Román, R. Sensing Parasites: Proteomic and Advanced Bio-Detection Alternatives. *J. Proteomics* **2016**, *136*, 145−156.
(55) Nethani, H.; Jangitwar, A.; Gupta, S.; Kandasubramanian, B.Silicone-Based Additive Manufacturing *Polym.-Plast. Technol. Mater.* 2024, pp 1−21 .
(56) Iftekar, S. F.; Aabid, A.; Amir, A.; Baig, M. Advancements and Limitations in 3D Printing Materials and Technologies: A Critical Review. *Polymers* **2023**, *15* (11), No. 2519.


https://doi.org/10.1021/acssensors.4c03306
*ACS Sens.* XXXX, XXX, XXX−XXX

(57) Gim, J.; Turng, L.-S. A Review of Current Advancements in High Surface Quality Injection Molding: Measurement, Influencing Factors, Prediction, and Control. *Polym. Test.* **2022**, *115*, No. 107718.
(58) Yang, L.; Luo, X.; Chang, W.; Tian, Y.; Wang, Z.; Gao, J.; Cai, Y.; Qin, Y.; Duxbury, M. Manufacturing of Anti-Fogging Super-Hydrophilic Microstructures on Glass by Nanosecond Laser. *J. Manuf. Processes* **2020**, *59*, 557−565.



https://doi.org/10.1021/acssensors.4c03306
*ACS Sens.* XXXX, XXX, XXX−XXX